Math. & Comput. Sci., 7(3) (2026), 88–96

Online: ISSN 2717-2708

Mathematics and Computational Sciences

Journal Homepage: http://mcs.qut.ac.ir/mcs

# Computational investigation of drag reduction on a large blunt Cone-Flare body in hypersonic turbulent flow using a Counter-Flow jet at various angle of attack

S. Aruna[a,*], M. Kayalvizhi[b], S.V. Anandhi[c], B. Amutha[a], N. Indumathi[d]

[a]Department of Mathematics, St.Joseph's College of Engineering, OMR, Chennai, 600 119, Tamilnadu, India.
[b]Department of Mathematics, Government Polytechnic, Daman, India.
[c]Department of Artificial Intelligence and Data Science, Ramco Institute of Technology, Rajapalayam, India.
[d]Department of Mathematics, Sri Ramakrishna Engineering College, Coimbatore, India.

## Abstract

The large blunt-nosed body is a common shape used in the design of hypersonic vehicles. The angle of attack ($\alpha$) in these vehicles introduces several challenges that can significantly affect performance. The primary issues caused by $\alpha$ in hypersonic vehicles include increased drag, thermal loads, flow separation, structural stress, control and stability difficulties, and complex shock wave interactions. Controlling $\alpha$ is critical for optimizing performance and preventing damage or failure during re-entry or high-speed manoeuvres. The current effort intends to minimise drag for a large blunt cone-flare body in hypersonic turbulent flow by maximising the angle of attack with a counter-flow jet. The massive blunt cone-flare body was simulated and the hypersonic flow conditions were set. The axisymmetric Navier–Stokes equations were numerically analysed using the shear stress transport model. Total drag, skin friction drag, and pressure drag were measured with and without the jet. Contours of Mach number and temperature were analysed to describe the flow pattern. Optimal jet conditions for drag mitigation were identified.

**Keywords:** Angle of Attack, Drag, Jet, Large Blunt.

**2020 MSC:** 35Q20, 76Lxx, 37C10, 37F05.



## 1. Introduction

Hypersonic vehicles operating at velocities exceeding Mach 5 are subjected not only to extreme aerodynamic heating but also to significant aerodynamic drag arising from strong shock waves, viscous dissipation, and high-temperature real-gas effects. At such high speeds, shock-induced compression dominates the flow field, leading to substantial pressure drag, particularly in the forebody region. Blunt-body configurations, commonly adopted for atmospheric re-entry vehicles due to their favorable thermal characteristics, inherently produce large bow shocks that increase drag while simultaneously intensifying stagnation-point heat loads. The trade-off between thermal protection and aerodynamic performance

*Corresponding author
Email addresses: arunas@stjosephs.ac.in (S. Aruna), gpdamankayalmaths@gmail.com (M. Kayalvizhi), anandhi@ritrjpm.ac.in (S.V. Anandhi), amuthab@stjosephs.ac.in (B. Amutha), indumathi.n@srec.ac.in (N. Indumathi)

doi: 10.30511/mcs.2026.2077646.1626

*Received: 14 November 2025 Accepted: 29 May 2026*

therefore remains a critical design challenge in hypersonic flight. To mitigate these adverse effects, various flow-control techniques have been explored, among which jet-based strategies have attracted considerable attention. Counterflow, lateral, and transpiration jets can significantly alter the shock structure and boundary-layer behavior ahead of the vehicle, resulting in a reduction of both aerodynamic heating and pressure drag. By creating a low-density, recirculating flow region in front of the blunt body, these jets effectively push the bow shock away from the surface, weakening shock strength and decreasing stagnation pressure. Consequently, jet-based drag reduction methods offer a promising avenue for enhancing hypersonic vehicle performance while complementing active thermal protection systems. Savino et al. (2005) [8, 9] constructed the flow field around a blunted cone-flare because it resembles the hypersonic flow around planetary entry vehicles. When assessing the surface heat flow, the area between the cone and the flare is very crucial. A numerical model was developed by taking the heating of the test model into account, and the numerical results showed a good agreement with the experimental results. Gerdroodbary et al. (2010) [5] carried out a numerical analysis of the effect of aerodisk/aerospike on large-angle blunt cones flying at hypersonic Mach number at different angles on drag reduction. Different lengths of spike were chosen in the analysis. The $k-\omega$ (SST) turbulence model was used to solve the compressible, three-dimensional complete Navier–Stokes equations for a free stream Mach number of 5.75. The results showed good agreement between the visualized shock structure and the computed drag on the blunt cone with aerospike. To reduce total drag over two cone-flare bodies in hypersonic turbulent flow at a Mach number of 6.5, Aruna et al. (2012) [1] conducted a computational study on the impact of jets. It was found that effective jet parameters brought notable reduction in drag. According to Li et al. (2016) [6], the opposing jet and varied blunt radii approach work well together to enhance the blunt waverider's aerodynamic performance. For a free stream Mach number of 5.75 at an altitude of 70 km, Arun Kumar et al. (2017) [2] examined the impact of aerospike shape on surface characteristics such as drag coefficient and convective heat transfer rate. Deng et al. (2018) [3] reduced drag in a hypersonic lifting-body model for Mach 8 flow at 40 km altitude by using the aerospike and counter-flowing jet principles. Wei et al. (2023) [4] used the computational fluid dynamics (CFD) approach to study aerodynamic drag reduction for vehicles with non-smooth surfaces. Shibin Luo et al. (2025) [7] numerically investigated the drag reduction and thermal protection efficiencies of combinational spike–jet configurations for various forebody geometries under hypersonic flow conditions. The analysis revealed that the synergy between the spike-induced separated region and the jet plume significantly alters the shock structure and reduces stagnation-point heating. The literature review highlights that drag is a significant issue during hypersonic flight, and various concepts such as energy deposition, aerospikes, counter-flow jets, and their combinations are employed to reduce it. Among these, the counter-flow jet is shown to offer efficient aerodynamic performance. These hypersonic flight challenges are explored through experimental work, numerical simulations, and the application of various soft computing techniques. In this study, a counter-flow jet is introduced at the blunt nose of a large blunt cone-flare body selected from existing literature in order to assess the effectiveness of the angle of attack. The objective of this study is to determine the optimal angle for the large blunt cone-flare body configuration that minimizes drag when a counter-flow jet is applied under specific flight conditions. The flow field around the blunt body is computed for a free stream Mach number of 6.5 at a height of 32.5 km. Numerical calculations are performed under various conditions, with and without a jet, to determine the flow field, pressure drag, skin friction drag, total drag, and static pressure distribution. These jet conditions include different angles of attack ($\alpha$) while keeping fixed jet parameters such as $p_{oj}$, $M_j$, $d/d_j$, and $T_{0j}$. The study also discusses the actual flow physics of this configuration with the jet, providing contour representations to illustrate the results.

## 2. Formulation of the problem

Figure 1 illustrates the counter-flow jet, which effectively reduces drag at the nose area by acting as an aerodynamic spike to separate the shock wave from the blunt nose and create a recirculation region.

Figure 2 depicts the large blunt cone-flare body. The body's blunt nose received the injection of the counter-flow jet.

The impact of the jet on minimizing overall drag on this blunt body was examined in a turbulent flow field while travelling at hypersonic speed at an altitude of 32.5 km.

### 2.1. *Configuration of cone flare body*

When a wide-angle flare section is added to the back end of the body, it functions as a spike, primarily helping to separate the flow and influencing the bow shocks in hypersonic flow.

This configuration is an axisymmetric model of length 3.957 m with a nose radius of 0.381 m and a body diameter of 3.3086 m.

The angle of the cone is 15° and the angle of the flare is 30°.

## 3. Solution of the Problem

The conservation form of the equations governing two-dimensional turbulent compressible flow based on the $k$–$\omega$ SST (Shear Stress Transport) model can be expressed as a set of transport equations that describe the conservation of mass, momentum, energy, and turbulence quantities. These equations account for the effects of compressibility and turbulence interactions within the flow field.

The model combines the advantages of both the $k$–$\epsilon$ and $k$–$\omega$ formulations, providing accurate predictions for boundary layer behaviour under adverse pressure gradients and separation.

In this form, the equations include terms representing convective and diffusive transport, along with source terms corresponding to turbulence production and dissipation. This formulation ensures that all relevant physical phenomena, such as viscous effects, compressibility, and turbulence dynamics, are consistently represented in a conservative framework suitable for numerical simulation of complex aerodynamic flows.

**Continuity equation:**

$$\nabla \cdot (\rho \vec{q}) = 0 \tag{3.1}$$

**Momentum equation:**

$$\nabla \cdot (\rho u \vec{q}) = -\frac{\partial p}{\partial x} + \frac{\partial \tau_{xx}}{\partial x} + \frac{\partial \tau_{yx}}{\partial y} + \rho f_x \tag{3.2}$$

$$\nabla \cdot (\rho v \vec{q}) = -\frac{\partial p}{\partial y} + \frac{\partial \tau_{xy}}{\partial x} + \frac{\partial \tau_{yy}}{\partial y} + \rho f_y \tag{3.3}$$

**Energy equation:**

$$\frac{\partial}{\partial x}\left(K\frac{\partial T}{\partial x}\right) + \frac{\partial}{\partial y}\left(K\frac{\partial T}{\partial y}\right) - \frac{\partial}{\partial x}(up) - \frac{\partial}{\partial y}(vp) + \frac{\partial}{\partial x}(u\tau_{xx}) + \frac{\partial}{\partial y}(u\tau_{yx}) + \frac{\partial}{\partial x}(v\tau_{xy}) + \frac{\partial}{\partial y}(v\tau_{yy}) + \rho\vec{f}\cdot\vec{q} = 0 \tag{3.4}$$

**Equation for turbulent kinetic energy ($k$):**

$$q_j\frac{\partial k}{\partial x_j} = P_k - \beta^* k\omega + \frac{\partial}{\partial x_j}\left[(\nu + \sigma_k \nu_T)\frac{\partial k}{\partial x_j}\right] \tag{3.5}$$

**Equation for specific dissipation rate ($\omega$):**

$$q_j\frac{\partial \omega}{\partial x_j} = \alpha S^2 - \beta^*\omega^2 + \frac{\partial}{\partial x_j}\left[(\nu + \sigma_\omega \nu_T)\frac{\partial \omega}{\partial x_j}\right] + 2(1-F_1)\sigma_{\omega 2}\frac{1}{\omega}\frac{\partial k}{\partial x_i}\frac{\partial \omega}{\partial x_i} \tag{3.6}$$

**where**

$\rho$ — density of the fluid in kg/m$^3$

$\vec{q}$ — velocity vector in m/s

$u$ and $v$ — velocity components in x and y directions respectively in m/s

$\vec{f}$ — force vector in N

$f_x$ and $f_y$ — body force components in x and y directions respectively in N

$k$ — Turbulent kinetic energy in m$^2$/s$^2$

$\omega$ — Specific dissipation rate in m$^2$/s$^3$

$T$ — Temperature of the fluid in K

$K$ — Thermal conductivity of the fluid in W/mK

$\nu$ — Kinematic viscosity in m$^2$/s

$\mu$ — Molecular viscosity coefficient

$$\tau_{xx} = \lambda(\nabla \cdot \vec{q}) + 2\mu \frac{\partial u}{\partial x} \tag{3.2}$$

$$\tau_{yy} = \lambda(\nabla \cdot \vec{q}) + 2\mu \frac{\partial v}{\partial y} \tag{3.3}$$

$$\tau_{xy} = \tau_{yx} = \mu \left[ \frac{\partial v}{\partial x} + \frac{\partial u}{\partial y} \right] \tag{3.4}$$

$$\lambda = -\frac{2}{3}\mu \tag{3.5}$$

$$P_k = \min\left( \tau_{ij} \frac{\partial q_i}{\partial x_j}, 10\beta^* k\omega \right) \tag{3.6}$$

$$S = \sqrt{2S_{ij}S_{ij}} \tag{3.7}$$

where

$$S_{ij} = \frac{1}{2}\left( \frac{\partial q_i}{\partial x_j} + \frac{\partial q_j}{\partial x_i} \right) \tag{3.8}$$

$$\nu_T = \frac{a_1 k}{\max(a_1\omega, SF_2)} \tag{3.9}$$

$$F_1 = \tanh\left\{ \min\left[ \max\left( \frac{\sqrt{k}}{\beta^*\omega y}, \frac{500\nu}{y^2\omega} \right), \frac{4\sigma_{\omega 2} k}{CD_{k\omega} y^2} \right] \right\} \tag{3.10}$$

$$F_2 = \tanh\left[\max\left(\frac{2\sqrt{k}}{\beta^* \omega y}, \frac{500\nu}{y^2\omega}\right)\right]^2 \tag{3.11}$$

$$CD_{k\omega} = \max\left(2\rho\sigma_{\omega 2}\frac{1}{\omega}\frac{\partial k}{\partial x_i}\frac{\partial \omega}{\partial x_i}, 10^{-10}\right) \tag{3.12}$$

$$\sigma_k = \frac{1}{\frac{F_1}{\sigma_{k1}} + \frac{(1-F_1)}{\sigma_{k2}}} \tag{3.13}$$

$$\sigma_\omega = \frac{1}{\frac{F_1}{\sigma_{\omega 1}} + \frac{(1-F_1)}{\sigma_{\omega 2}}} \tag{3.14}$$

$a_1$, $\sigma_{k1}$, $\sigma_{k2}$, $\sigma_{\omega 1}$, $\sigma_{\omega 2}$, $\alpha$, and $\beta^*$ are constants and they are given by: In the method of analysis, *Fluent*

Table 1: Constants used in the k–ω SST model

| $a_1$ | $\sigma_{k1}$ | $\sigma_{k2}$ | $\sigma_{\omega 1}$ | $\sigma_{\omega 2}$ | $\alpha$ | $\beta^*$ |
|---|---|---|---|---|---|---|
| 0.31 | 1.176 | 1 | 2 | 0.856 | 0.52 | 0.09 |

*6.3.26* was used to obtain the numerical solutions. In the $x$ direction, there are 108 grid points, and in the $y$ direction, there are 290.

Figure 3 displays the boundary conditions used for this investigation.

For this study, the ROE-FDS (Roe Flux-Difference Splitting Scheme) was selected. Additionally, the $k$–$\omega$ shear stress transport model was chosen as the turbulence model.

The solution was marched with an initial Courant number of 0.5, which was progressively raised to 0.7, and the entire flow field was initialized with the free-stream conditions.

The convergence criterion for the solution was set to $1.0 \times 10^{-6}$. Convergence was observed after approximately 48,000 iterations at a Courant number of 2.

## 4. Results and Discussion

The flow patterns are vividly illustrated through contour representations. The following sections present the Mach number contours for the specified values of $p_{0j}$, $d/d_j$, $M_j$, and various $\alpha$, while maintaining $T_{0j} = 300$ K, both with and without a jet.

### 4.1. *Results in the absence of jet*

#### 4.1.1. *Contour representations in the absence of jet*

From Figure 4, it is clearly observed that the Mach number near the wall region of the body is low, which leads to an increase in overall drag. A detached shock wave is also captured at the inception of the flare in the absence of a jet. The figure vividly shows the effect of angle of attack ($\alpha$) on the Mach number contours for increasing values of $\alpha$. As $\alpha$ increases, the velocity near the wall region decreases, thereby increasing the drag for higher values of $\alpha$.

#### 4.1.2. *Numerical results*

The numerical findings for various values of $\alpha$ in the absence of a jet are presented in Table 1. From the table analysis, the influence of $\alpha$ results in a slight rise in skin friction drag for $\alpha = 2°$, which subsequently increases as $\alpha$ grows. A significant decrease in skin friction drag is observed for $\alpha = 10°$. There is no noticeable variation, as pressure drag and total drag both increase with increasing $\alpha$.

*4.2. Graphical illustrations*

Numerical results are obtained for different values of $\alpha$ ($\alpha = 0°, 2°, 4°, 6°, 8°$, and $10°$) without a jet. The influence of $\alpha$ on static pressure is illustrated in Figure 5, and it is evident that the static pressure across the body increases with increasing $\alpha$.

*4.3. Results in the presence of jet*

*4.3.1. Contours of Mach number*

When $M_j = 1$, $d/d_j = 10$, $p_{0j} = 300$ kPa, and $T_{0j} = 300$ K, Figure 6 clearly illustrates how the angle of attack ($\alpha$) affects the Mach number contours for increasing values of $\alpha$ in the presence of a jet. The jet response decreases as $\alpha$ increases, resulting in a reduction in velocity in the vicinity of the wall region.

*4.3.2. Numerical results for various $\alpha$ in the presence of jet*

Table 2 presents the numerical results for different values of $\alpha$ in the presence of a jet for fixed values of $M_j = 1$, $d/d_j = 10$, $p_{0j} = 300$ kPa, and $T_{0j} = 300$ K. When compared with Table 1, the effect of angle of attack results in a considerable reduction in drag for $\alpha = 2°$. It is clearly observed that as $\alpha$ increases, pressure drag, skin friction drag, and total drag also increase, except for $\alpha = 2°$. Therefore, $\alpha = 2°$ yields the optimum solution for drag reduction in the presence of a jet.

*4.3.3. Graphical illustrations*

For the case with a jet, numerical results are obtained for various values of $\alpha$ corresponding to $M_j = 1$, $d/d_j = 10$, $T_{0j} = 300$ K, and $p_{0j} = 300$ kPa. Figure 7 shows the effect of $\alpha$ on static pressure, and it is observed that static pressure over the body increases with increasing $\alpha$.

## 5. Conclusion

The following conclusions are drawn from the aforementioned findings and are summarized below:

1. In the present work, the Navier–Stokes equation and energy equation with variable viscosity were solved using the $k$–$\omega$ SST turbulence model over a cone-flare body for both the absence and presence of a jet in large blunt cone-flare configurations. This enabled CFD solutions of the turbulent flow field.
2. It is evident that applying an opposing jet effectively reduces total drag and skin friction drag in hypersonic flow.
3. Several efficient jet conditions were identified through the examination of various opposing jet conditions in hypersonic turbulent flow.
4. At $p_{0j} = 300$ kPa, $d/d_j = 10$, $M_j = 1$, and $T_{0j} = 300$ K, $\alpha = 2°$ produced a greater reduction in pressure drag, skin friction drag, and total drag.
5. It is noteworthy that, when compared with the case without a jet, the presence of a jet reduces pressure drag by 37.29%, skin friction drag by 92.23%, and total drag by 37.92%.
6. Figures and Tables

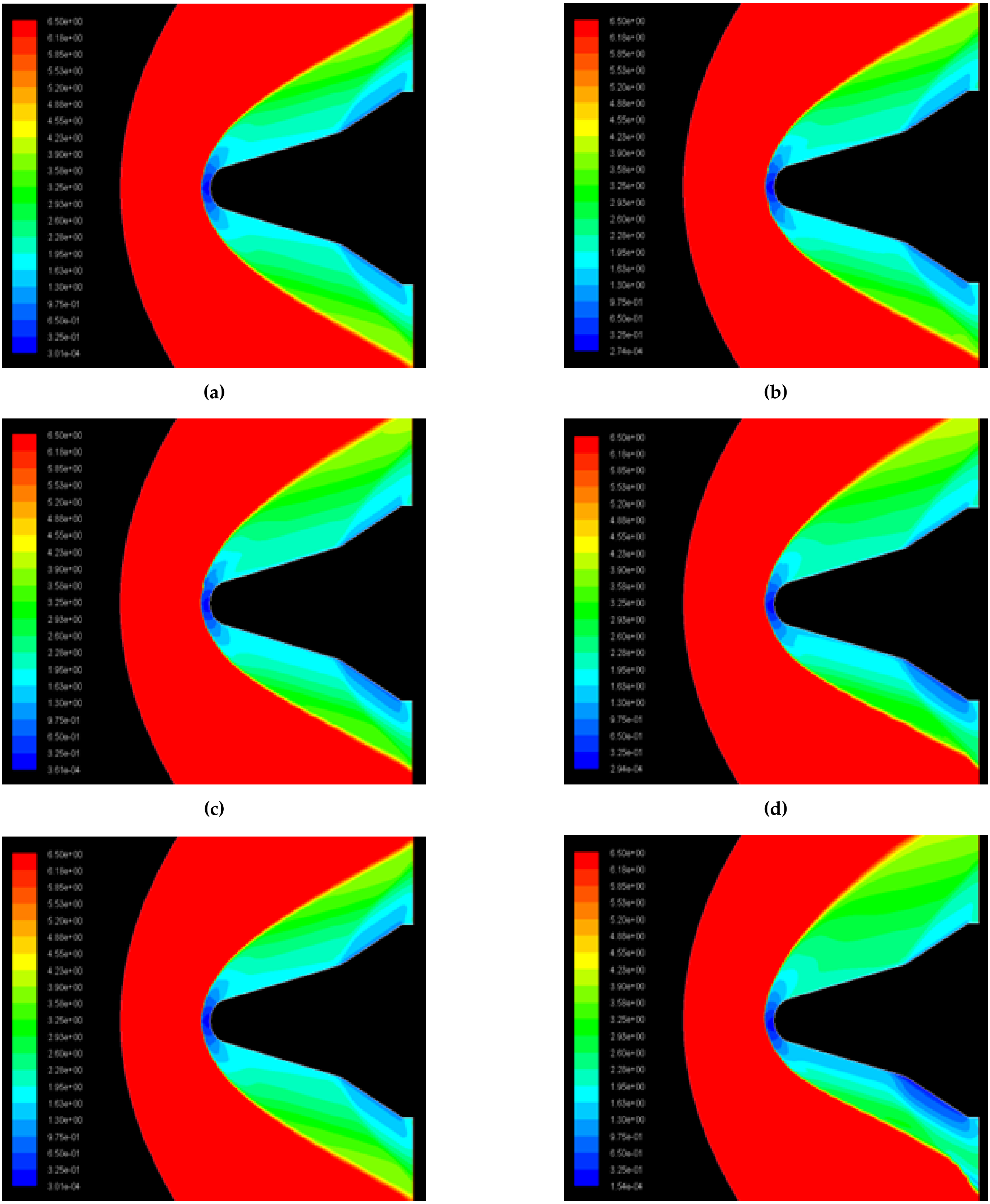

**(a)** **(b)** **(c)** **(d)** **(e)** **(f)**

Figure 1: Contours of Mach Number for various $\alpha$ in the absence of jet. In Figure 4, a, b, c, d, e, f denotes the contours when $\alpha = 0, 2, 4, 6, 8$ respectively.

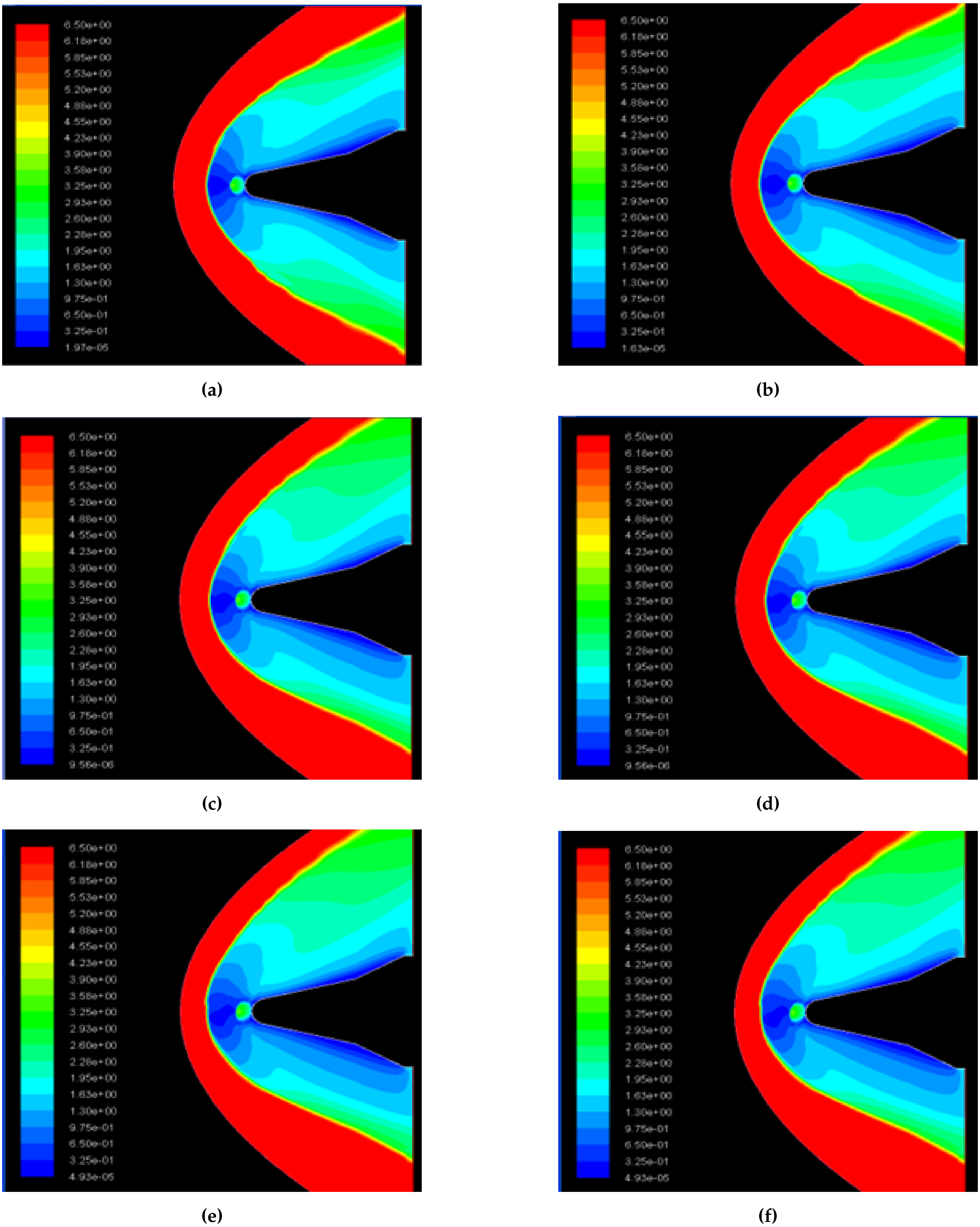


**(a)** **(b)** **(c)** **(d)** **(e)** **(f)**

Figure 2: Contours of Mach Number for various $\alpha$ in the presence of jet. In Figure 4, a, b, c, d, e, f denotes the contours when $\alpha = 0, 2, 4, 6, 8$ respectively.

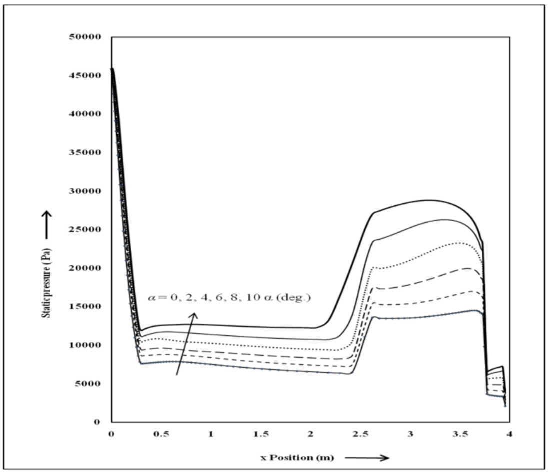


Figure 3: Static Pressure Distribution for various α in the presence of jet

Table 2: For various α in the absence of jet

| α in Degree | Drag of pressure in N | Drag from skin friction in N | Drag total in N |
|---|---|---|---|
| 0 | 52440.79 | 608.38 | 53049.17 |
| 2 | 52727.75 | 611.78 | 53339.53 |
| 4 | 53570.36 | 602.03 | 54172.39 |
| 6 | 54954.13 | 582.58 | 55536.72 |
| 8 | 56609.61 | 554.09 | 57163.70 |
| 10 | 58872.78 | 525.07 | 59397.85 |

Table 3: For various α in the presence of jet

| α in Degree | Pressure drag in N | Drag from skin friction in N | Drag total in N |
|---|---|---|---|
| 0 | 33077.50 | 56.73 | 33134.23 |
| 2 | 32885.94 | 47.23 | 32933.17 |
| 4 | 33791.29 | 51.48 | 33842.77 |
| 6 | 34195.38 | 51.76 | 34247.14 |
| 8 | 34936.57 | 53.33 | 34989.90 |
| 10 | 36681.01 | 57.58 | 36738.58 |

## References


[1] Aruna, S., Anjali Devi, S. P. (2012). Procedia Engineering, 38, 3635–3643. 1

[2] Chinnappan, A. K., Malaikannan, G., Kumar, R. (2017). Aerospace Science and Technology, 66, 119–129. 1

[3] Deng, F., Xie, F., Qin, N. (2018). Aerospace Science and Technology, 76, 361–372. 1

[4] Gao, W., Wei, M., Huang, S. (2023). Proceedings of the Institution of Mechanical Engineers, Part D: Journal of Automobile Engineering, 238(9), 1–15. 1

[5] Gerdroodbary, M. B., Hosseinalipour, S. M. (2010). Acta Astronautica, 67, 180–193. 1

[6] Li, S.-B., Wang, Z.-G., Barakos, G. N., Huang, W., Steijl, R. (2016). Acta Astronautica, 127, 120–134. 1

[7] Luo, S., Li, D., Wang, J., Dai, Y., Feng, Y. (2025). Drag reduction and thermal protection efficiencies of combinational spike and opposing jet with different forebody geometries in hypersonic flows. Applied Thermal Engineering, 278, 127298. 1

[8] Savino, R., Paterna, D. (2005). Computers & Fluids, 34, 859–878. 1

[9] Schrijer, F. F. J. (2003). Transient heat transfer measurements in a short duration hypersonic facility on a blunted cone-flare using QIRT (Doctoral dissertation, Delft University of Technology). 1